75

SOCIETY OF AUTOMOTIVE ENGINEERS, INC.
400 Commonwealth Drive, Warrendale, Pa. 15096

Time Resolved Measurements of Exhaust Composition and Flow Rate in a Wankel Engine

Colin R. Ferguson, Guido A. Danieli,
John B. Heywood, and James C. Keck
Massachusetts Institute of Technology

SOCIETY OF AUTOMOTIVE ENGINEERS

Automotive Engineering Congress and Exposition
Detroit, Michigan
February 24-28, 1975

750024

750024

Time Resolved Measurements of Exhaust Composition and Flow Rate in a Wankel Engine

Colin R. Ferguson, Guido A. Danieli, John B. Heywood, and James C. Keck
Massachusetts Institute of Technology

ABSTRACT

Measurements were made of exhaust histories of the following species: unburned hydrocarbons (HC), carbon monoxide, carbon dioxide, oxygen, and nitric oxide (NO). The measurements show that the exhaust flow can be divided into two distinct phases: a leading gas low in HC and high in NO followed by a trailing gas high in HC and low in NO. Calculations of time resolved equivalence ratio throughout the exhaust process show no evidence of a stratified combustion.

The exhaust mass flow rate is time resolved by forcing the flow to be locally quasi-steady at an orifice placed in the exhaust pipe. The results with the quasi-steady assumption are shown to be consistent with the measurements. Predictions are made of time resolved mass flow rate which compare favorably to the experimental data base.

The composition and flow histories provide sufficient information to calculate the time resolved flow rates of the individual species measured. The information so generated shows most of the NO is exhausted with the leading gas while most of the HC is exhausted with the trailing gas.

COMBUSTION IN THE WANKEL ENGINE has been studied both theoretically and experimentally (1–5).* While in principle flame propagation in the engine is similar to a piston engine, the Wankel geometry allows nonequilibrium effects to become more significant. The high surface-to-volume ratios and rotating combustion chambers put a significant fraction of the working fluid into boundary layers, particularly for gases which burn in the regime of top dead center (tdc); the temperature history of such gases is significantly lower than that predicted by a model assuming isenthalpic combustion and isentropic compressions and expansions (3). Near tdc the rotor and the housing form a nozzlelike restriction through which the gases flow at high velocity such that the local heat transfer coefficient may be as much as three times the average.

*Numbers in parentheses designate References at end of paper.

Observations of flame propagation (4,5) show that the speed of the flame is assisted in the direction of rotor rotation and impeded in the opposite direction. It is believed that these gas motions which affect flame propagation may also affect fuel distribution within the engine. Yamamoto (6) shows that carbon monoxide emissions as a function of equivalence ratio are significantly different from equilibrium predictions and so concludes that the combustion is stratified.

This study examines fluid motions within the engine by experimentally time resolving the exhaust composition and mass flow rate. Similar studies performed on a piston engine (7) have shown the exhaust gas to possess distinct nonuniformities in the unburned hydrocarbon concentrations (HC). Mass flow experiments by Tabaczynski et al (8) cataloged the mechanisms behind the nonuniformities. The HC emissions exit the cylinder in two distinct peaks. The first peak occurs during blowdown and is presumed to be an entrainment of the cylinder

head quench layer. The second peak occurs as the piston approaches tdc and results from a vortex motion set up by the piston scraping the hydrocarbon-rich boundary layer from the cylinder wall.

Similar experiments have been performed on the Wankel (2) but not enough data was taken to examine the hypothesized stratified combustion. Therefore our study time resolves the HC, carbon monoxide (CO), carbon dioxide (CO_2), and oxygen (O_2) exhaust concentrations. This information is sufficient to determine a time resolved equivalence ratio.

The exhaust mass flow rate is time resolved and compared to predictions of a previously developed model. Since a quantitative understanding of nitric oxide (NO) emissions from the engine has not yet been demonstrated, the NO emissions are also time resolved.

The paper is divided into essentially two sections: a description of the principles and techniques underlying the experiments, and the presentation and analysis of the resultant data.

EXPERIMENT: TECHNIQUES AND PRINCIPLES

MASS FLOW MEASUREMENTS–Instantaneous mass fluxes from the engine have been measured by forcing the flow to be locally quasi-steady at an orifice mounted downstream of the exhaust port as shown in Fig. 1. Eq. 1 describes the flow through the orifice when the flow is quasi-steady:

$$\dot{m}_E = C_d A_2 \frac{P_o}{RT_o}\sqrt{\gamma RT_o}\sqrt{\frac{2}{\gamma-1}\left[\left(\frac{P_2}{P_o}\right)^{2/\gamma}-\left(\frac{P_2}{P_o}\right)^{\gamma+1/\gamma}\right]} \quad (1)$$

where:

C_d = discharge coefficient
A_2 = area of orifice
R = specific gas constant
γ = specific heat ratio
P_o = stagnation pressure
T_o = stagnation temperature
P_2 = static pressure at orifice

Time resolved temperatures have been measured in piston engine exhausts (8), but in this work the stagnation temperature is calculated by the model detailed in Ref. 3. Basically the model integrates simultaneously the equations of state and energy conservation for an open system of the time-varying volume corresponding to the walls of the exhausting chamber. The mass flow leaving that chamber is assumed to be a quasi-steady one dimensional flow. The state variables corresponding to pressure and temperature within the chamber are the solutions to what is an initial value problem. That temperature is assumed to be the stagnation temperature necessary for the measurement. The mass flow rate measured according to Eq. 1 is weakly dependent upon the temperature so that errors in such an approach are small.

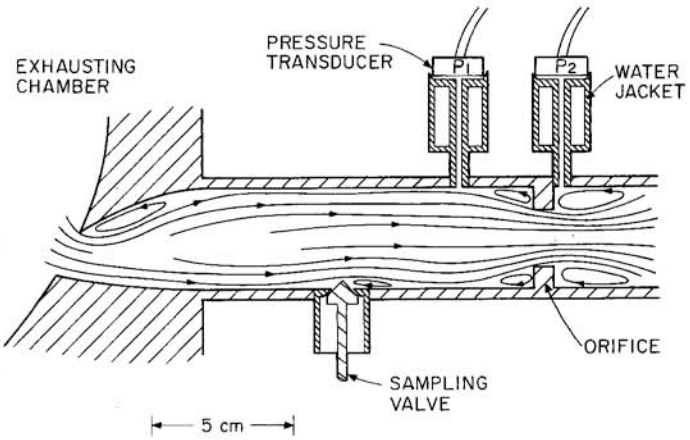

Fig. 1 – Schematic of test section for measurements of mass flow rate and composition

Stagnation pressure is determined by an iteration. Starting with $P_o = P_1$ (the static pressure upstream of the orifice), the mass flow rate is calculated according to Eq. 1. The upstream static temperature (T_1) is assumed equal to the stagnation temperature and the Mach number upstream is:

$$M_1 = \frac{RT_1}{P_1}\frac{\dot{m}_E}{A_1}\frac{1}{\sqrt{\gamma RT_1}} \quad (2)$$

The stagnation pressure:

$$P_o = P_1\left(1+\frac{\gamma-1}{2}M_1^2\right)^{\gamma/\gamma-1} \quad (3)$$

and upstream static temperature:

$$T_1 = T_o\left(1+\frac{\gamma-1}{2}M_1^2\right)^{-1} \quad (4)$$

are reevaluated and the process iterated. Convergence is rapid since the upstream Mach number is small.

Eq. 1 assumes the flow upstream of the orifice is a quasi-steady and isentropic flow of an ideal gas. Such an approach is consistent with detailed studies by Benson and his co-workers (for example, see Ref. 9) who concluded that the nonisentropic flow downstream of such an orifice did not significantly affect upstream events.

The flow will be quasi-steady if the temporal changes in the flow field are small compared to the convective changes. The assumptions made are thus:

$$\frac{\partial\rho}{\partial t} \ll u\frac{\partial\rho}{\partial x} \quad (5)$$

$$\frac{\partial p}{\partial t} \ll u\frac{\partial p}{\partial x} \quad (6)$$

$$\frac{\partial u}{\partial t} \ll u\frac{\partial u}{\partial x} \quad (7)$$

where:

$\frac{\partial}{\partial t}$ = temporal operator

$u\frac{\partial}{\partial x}$ = convective operator

u = velocity

density

The discharge coefficient in Eq. 1 accounts for multidimensional effects. Two orifices were used in the experiments and were calibrated by mounting the test section of Fig. 1 downstream of an ASME orifice (10) and passing steady flow air through the system. The larger orifice was 2.54 cm in diameter and $C_d = 0.86$ while the smaller orifice was 1.91 cm in diameter and $C_d = 0.75$. The larger orifice had a larger discharge coefficient because it was beveled on the upstream side. The calibrations on the small orifice were performed by varying the Reynolds number based on orifice diameter from 3.8×10^4 to 4.2×10^5. Simultaneously the Mach number at the throat varied from 0.22 to 1.00 and the pressure ratio (P_o/P_2) varied from 1.03 to 2.16. All the C_d measured fell within ±5% of the constant discharge coefficient value given above.

The gas constant and specific heat ratio were determined from curves fitted to equilibrium calculations performed at a temperature of 1200°K and a pressure of 101 kPa. The resultant curves fitted by collocation give the molecular weight:

$$MW = -371.623 + 1421.94\,\phi - 1876.09\,\phi^2 + 1091.66\,\phi^3 - 237.276\,\phi^4 \quad (8)$$

and the specific heat ratio, γ, of the exhaust products as functions of the equivalence ratio for combustion of isooctane and air:

$$\gamma = -0.0935211 + 5.10914\,\phi - 6.96955\,\phi^2 + 4.14715\,\phi^3 - 0.912124\,\phi^4 \quad (9)$$

Eqs. 8 and 9 are valid only for fuel-rich combustion. The gas constant is equal to the universal gas constant divided by the molecular weight.

TIME RESOLVED COMPOSITION MEASUREMENT– Composition of the exhaust gas at a given angle was measured by withdrawing for analysis a small exhaust sample at the same point in the exhaust process from successive cycles. This was accomplished by a sampling valve mounted downstream of the exhaust port. By varying the angle at which sampling occurred, the composition was discretely time resolved.

The sampling valve (Fig. 2) was designed and built by Tabaczynski (11). The controls have since been redesigned to allow the operator to open the valve at 1/2 or 1/4 the engine cycle frequency for sampling at high engine speeds. The valve was adjusted so that its open time was 2 ms.

The design of the valve was such that the sample was sealed from the atmosphere by a labyrinth seal around the shaft. Leakage through that seal, while small, must be known to correct the measured species concentrations.

The leakage correction to oxygen data is:

$$[O_2]_c = [O_2]_w\left(1 + \frac{Q_a}{Q_s}\right) - 0.21\,\frac{Q_a}{Q_s} \quad (10)$$

where:

Q_a/Q_s = ratio of leakage airflow to sample flow
$[O_2]_c$ = corrected concentration of O_2
$[O_2]_w$ = measured (wet) concentration of O_2

By requiring that:

$$\frac{\delta \dot{m}_E [O_2]_c d\theta}{\delta \dot{m}_E d\theta} = [O_2]_{ave} \quad (11)$$

where:

δ = cyclic integral
$d\theta$ = differential crank angle
$[O_2]_{ave}$ = measured (wet) average O_2 concentration

the leakage correction factor (Q_a/Q_s) was determined, and was always less than 5% in these experiments. Integrations such as Eq. 11 for leakage corrected data of other species yielded values within ±10% of the measured average values.

The sample was pulled through the valve by a metal bellows MB-21-HT pump and passed through a heated sampling line

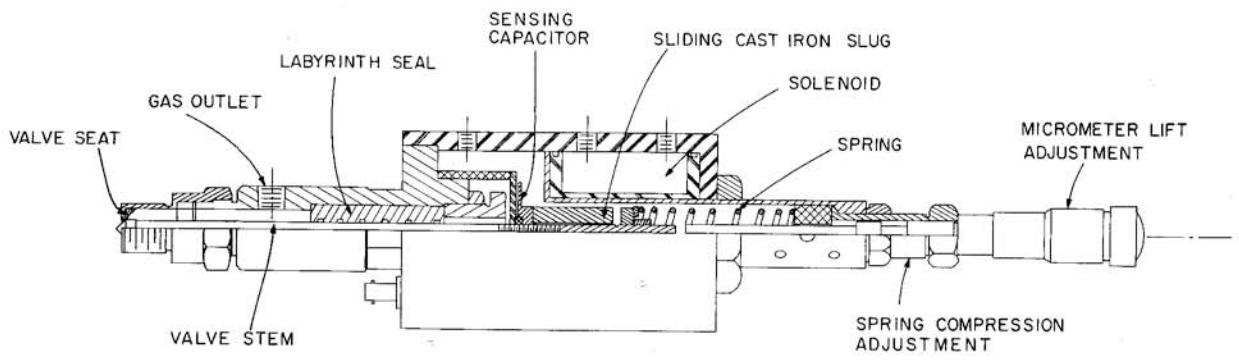

Fig. 2 – Assembly drawing of sampling valve, from Reference 11

and filter to a Scott model 215 heated total HC analyzer. The bypass of the HC analyzer was then dried and delivered to the following instruments for analysis: TECO model 10A chemiluminescent NO analyzer, Scott model 150 paramagnetic O_2 analyzer, Beckman model 315A NDIR CO_2 analyzer, and a Beckman model 864 NDIR CO analyzer. Sampling flow rate was of order 800 cm^3/min at STP.

It has long been recognized that the average exhaust composition is a function of the equivalence ratio. Thus it is natural to assume that a time resolved equivalence ratio may be calculated from time resolved composition. On that assumption time resolved equivalence ratios were calculated by the model presented in Ref. 12.

There it was assumed that the exhaust gas may be divided into a burned fraction plus an unburned fraction. The model fit one undetermined constant to direct measurements of air-fuel ratios. The constant was defined by:

$$K = \frac{[H_2O]\,[CO]}{[CO_2]\,[H_2]} \tag{12}$$

A carbon balance and an oxygen balance performed on a combustion equation including unburned hydrocarbons in the burned gas showed that the equivalence ratio was:

$$\phi = \frac{\left(1+\frac{1}{4}\frac{m}{n}\right)([CO_2] + [CO] + [HC])}{[CO_2] + \frac{1}{2}[H_2O] + \frac{1}{2}[CO] + [O_2]} \tag{13}$$

where m/n is the ratio of hydrogen to carbon atoms in the fuel and HC must be counted by carbon atoms in the exhaust HC. What Spindt (12) did in effect was determine an empirical correlation for the exhaust water concentration:

$$[H_2O] = \frac{1}{2}\frac{m}{n}([CO_2] + [CO])/\left(\frac{1}{3.5}\frac{[CO]}{[CO_2]} + 1\right) \tag{14}$$

which follows from a hydrogen balance assuming that the ratio of hydrogen to carbon atoms in the exhaust HC is the same as that of the fuel. Eqs. 12–14 are mathematically equivalent to Spindt's; however, they are simpler because his assumption that the exhaust gas consists of a burned fraction plus an unburned fraction is more restrictive than necessary.

The concentrations in Eqs. 12–14 are wet and the constant, 3.5, is the undetermined constant of Eq. 12. On that basis equivalence ratios have been calculated and the concentrations measured dry have been corrected to a wet basis.

EXPERIMENTAL CONDITIONS–The experiments were performed on a Toyo Kogyo series 10A engine (4) run at manufacturer's specified operating conditions; the distributors controlled the spark timing, and the carburetor set the flow rates of fuel and air delivered to the engine. The general characteristics of the engine are outlined in Table 1. The engine was lubricated with Texaco URSA oil LA-23 and fueled with isooctane. The data analyzed came from the matrix of engine operating parameters shown in Table 2.

To mount the sampling valve and exhaust orifice, a water-cooled test section replaced the exhaust header. The exhaust port, a copper gasket, and the test section were carefully matched so that the flow saw no surface discontinuities. Pressures P_1 and P_2 were measured with TYCO model AB strain gage pressure transducers mounted in water-cooled adapters as shown in Fig. 1.

The chamber pressure was recorded with a PCB model 111A24 piezoelectric pressure transducer mounted on the leading spark plug. The transducer spark plug adapter system provided by PCB was not adequate for accurate pressure measurements since attenuation of the pressure signal apparently occurred. The calibration of the pressure measuring system was therefore accomplished by forcing the integral of PdV over the cycle to be equal to the average work measured by the dynamometer. The pressure records so obtained were estimated to be accurate to about ±5%. Our crank angle measurements were accurate to ±1 crank angle deg.

To measure the time averaged fuel flow delivered to the engine a Floscan model 200A electronic totalizer was coupled to a clock. Airflow into the engine was determined from the fuel-air ratio calculated from exhaust gas analysis (12) and fuel flow measurements.

RESULTS AND THEIR INTERPRETATION

Fig. 3 shows exhaust pressure data taken with the engine running at 1500 rpm and a bmep ≈390 kPa (57 psi). The upper curve was P_1-P_2 (Fig. 1) from the large orifice, while the lower curve was from the small orifice. The large orifice was too big to force most of the flow to be quasi-steady under the aforementioned conditions, thus pressure gradients across the orifice were set up by the unsteady flow. The period of the resulting wave forms, nondimensionalized with the exhaust pipe length (1.25 m) and the average stagnation sound speed, was approximately five. One dimensional order-of-magnitude

Table 1 – Toyo Kogyo Engine Specifications

Type	Rotary piston engine, in line, 2 rotor, water-cooled
Displacement	491 cm^3 X 2 rotors (29.96 in^3 X 2 rotors)
Compression ratio	9.4:1
Compression pressure	6.0 kg/cm^2 at 280 rpm (85 lb/in^2 at 280 rpm)
Max. brake hp	110 hp/7000 rpm (SAE)
Max. torque	100 ft-lb/4000 rpm (SAE)
Port timing:	
Intake opens	Primary: 32 deg atdc Secondary: 32 deg atdc
Intake closes	Primary: 40 deg abdc Secondary: 40 deg abdc
Exhaust opens	75 deg bbdc
Exhaust closes	35 deg bbdc

Table 2 – Major Engine Operating Parameters

Engine Speed, rpm	bmep, kPa	fmep, kPa	Leading Spark, deg btdc	Trailing Spark, deg btdc	ϕ	CO, %	CO_2, %	O_2 %	HC, ppmC	NO, ppm	Fuel Flow, g/s
1000	173	116	−18	−14	1.11	1.3	9.5	2.6	22500	220	0.897
1000	373	169	−10	+3	1.05	1.6	9.9	2.4	15000	642	1.12
1500	386	142	−10	−1	1.04	1.2	9.8	2.3	15250	1064	1.42
1500	399	142	−10	−1	1.12	2.7	9.1	2.0	16250	453	1.49
2000	427	133	−10	0	1.03	1.2	10.1	2.0	12150	1025	1.75
2000	427	133	−10	0	1.04	1.3	10.3	2.0	12000	1119	1.75
2000	584	162	−20	−12	1.09	2.8	10.1	1.6	9400	669	2.68

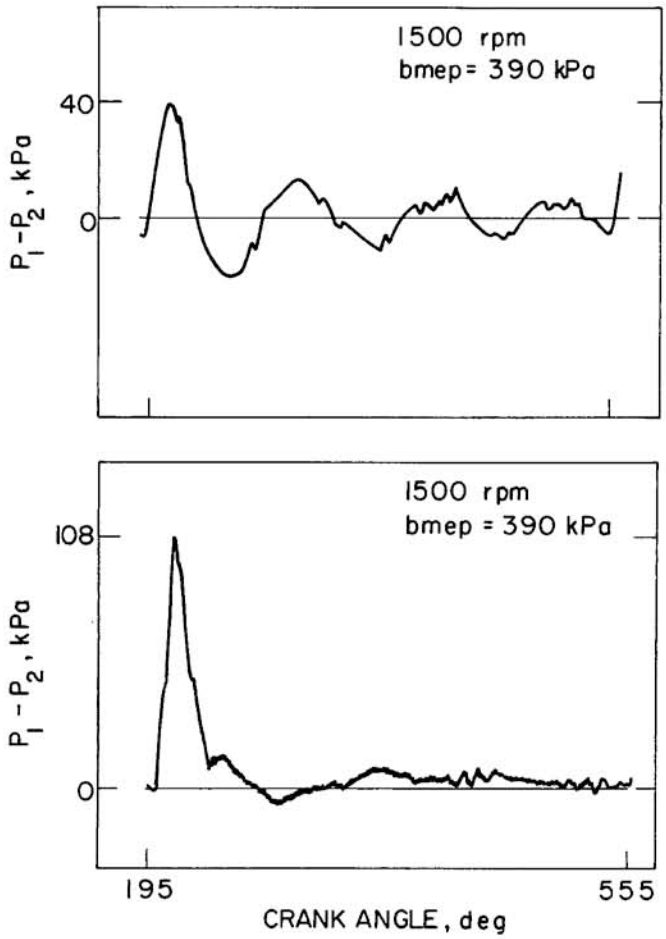

Fig. 3 – Pressure difference at large orifice (upper) and at small orifice (lower) for 1500 rpm and bmep = 390 kPa. The exhaust port opens at 195 deg and starts closing at 555 deg

analysis of the unsteady flow predicted a nondimensional period of four.

The small orifice on the other hand was small enough to time resolve most of the mass flow rate according to Eq. 1. Fig. 4 shows measured and predicted mass flow rates for three different runs. The port opened and for a few degrees of crank revolution the flow was unsteady as it tried to overcome inertial resistance and establish a steady state. The flow rapidly reached a quasi-steady state and the exhausting chamber quasi-steadily blew down to the exhaust pressure. For the runs analyzed the port timing was not optimum, thus blowdown was complete before bottom dead center (bdc). The expanding volume then drew exhaust gas back into the engine until bdc. After bdc the gas was incompressibly pushed out of the chamber until tdc, where a small backflow was started and continued until the port closed.

From the predicted exhaust flow histories, finite difference estimates have been made to check the quasi-steady assumptions. It was found that the criteria were violated only as the

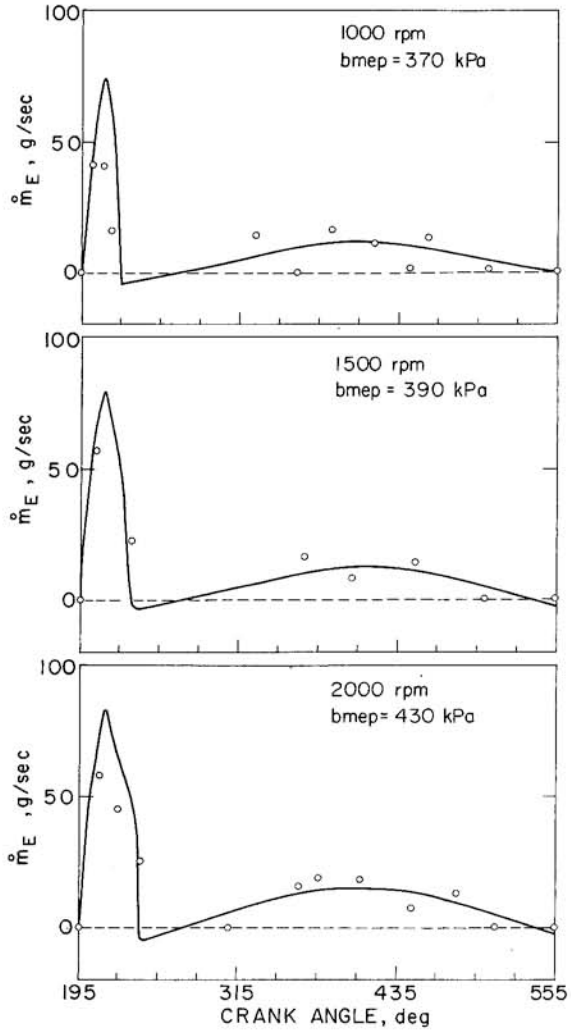

Fig. 4 – Comparison of measured (points) and predicted (curve) exhaust flow rates at bmep ≈400 kPa and 1000 rpm (upper), 1500 rpm (middle), and 2000 rpm (lower)

exhaust velocity approached zero and that Eq. 7 was the more critical criterion. For the flow histories studied the integrated errors were small enough to be unimportant.

Experimentally the backflows could not be measured with the pressure data obtained because P_1 was now measured in a region which was nonisentropic. The blowdown was easy to resolve, though there was some doubt about the transducers' ability to follow the pressure history at this time since their natural frequency was only 4500 Hz. During the incompressible phase, the pressure signal-to-noise ratios were low; this was responsible for the scattering of the experimental points in this regime. The noise was presumed to arise primarily from acoustical oscillations in the transducer passages (for example, see Ref. 13, problem 23.6).

Overall the agreement between the experimental points and the predicted curves was good. Although limitations existed in both the model and the experiment, and better agreement would have been fortuitous, it must be recognized that steady flow discharge coefficients are functions of Reynolds numbers, Mach numbers, and pressure ratios through the restrictions; unsteady discharge coefficients deviate from steady state values; the model assumes pressure recovery many diameters downstream of the exhaust port; transducer response may be less than ideal; and finally the model is sensitive to the rate at which the port opens. In our study the port was modeled as linearly opening to an area of 4.84 cm^2 (C_d = 0.75) in 20 crank angle deg.

Since both the sampling valve and the orifice were not located at the exhaust port inlet, corrections were made to determine events at the exhaust port. As the port opened, it exposed the high pressure exhausting chamber to the low pressure exhaust pipe. The flow downstream of the port at the orifice lagged the flow at the port. The delay was assumed constant and equal to the measured difference between the angle of first pressure rise at the upstream pressure tap (P_1) and the angle at which the exhaust port opened (195 deg). The delays so measured were small (~10 deg). The actual delay was not time invariant and was a complicated function of gas speed, sound speed, and the transducer adapters' fluidic capacitance.

Particle trajectories were calculated from the predicted mass flow curves by assuming a plug flow in the exhaust pipe. Fig. 5 illustrates the procedure. The distance coordinate refers to distance downstream of the exhaust port inlet; zero distance corresponds to the inside housing surface. The line labeled S.V. is the position at which the sampling valve is located in an exhaust pipe of constant area, that is, the length scale has been modified to account for the area change from the port inlet to the sampling valve.

The trajectories (path lines) are calculated by integrating velocity histories of fluid elements exhausted at different times during the cycle. By assuming that the mass flow is everywhere the same between the sampling valve and the port inlet (plug flow) an estimate may be made of the time required for an exhausted element to reach the sampling station. In Fig. 5 most particles leave the engine and reach the sampling valve in a short time compared to the cycle period. Thus relaxation of

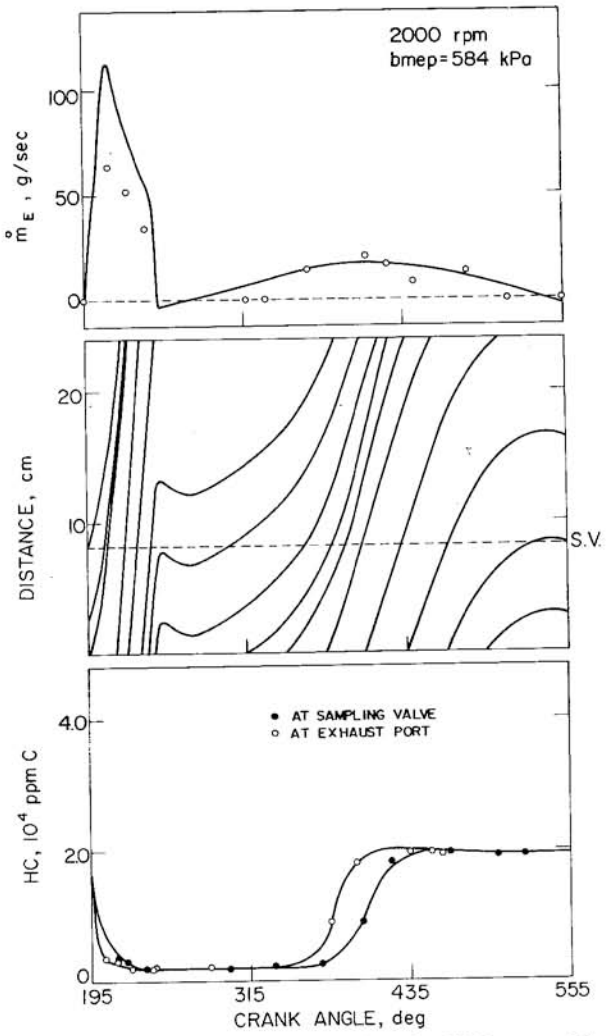

Fig. 5 – Illustration of trajectory corrections for 2000 rpm and bmep = 584 kPa

nonuniformities such as measured in Ref. 7 have been minimized. (It is important to note that the trajectory corrections neglect mixing between fluid elements. It will be shown later that mixing during blowdown is significant.) With but one exception, all the trajectory corrections are typified by Fig. 5 so that measurements made at the sampling station are indeed representative of histories at the exhaust port.

The experiment performed at 1000 rpm and bmep = 173 kPa proved to be the only case in which the trajectory corrections were large and inconsistent with the experimental observations. Fig. 6 illustrates the direct application of the aforementioned trajectory correction to the HC history measured at the sampling valve. There is a lot of backflow into the engine and a relatively long time during which the flow is not quasi-steady. During this part of the cycle the HC concentration at the sampling valve is oscillating. This results when the trajectory of the first element exhausted crosses the sampling valve position more than once as the flow sloshes back and forth. The trajectory which starts at the housing at 195 crank angle deg after tdc represents the positional history of an imaginary surface separating the HC-laden gas exhausted near the end of the previous cycle and the relatively HC-free gas first exhausted

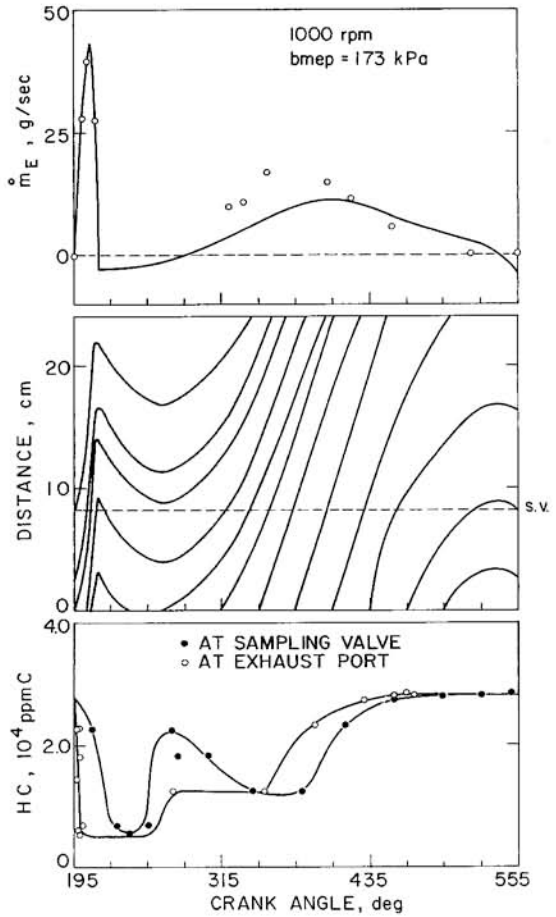

Fig. 6 – Illustration of trajectory corrections for 1000 rpm and bmep = 173 kPa

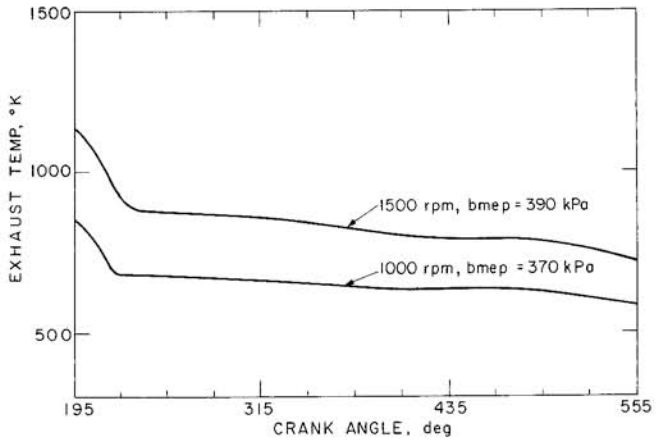

Fig. 7 – Calculated exhaust temperature for bmep = 390 kPa, 1500 rpm (upper) and bmep = 370 kPa, 1000 rpm (lower)

in the new cycle. From the observed oscillations of HC concentration at the sampling valve it is clear that the imaginary surface passes the sampling valve more than once per cycle whereas the calculated trajectory does not. The shape of the resultant curve is, however, qualitatively correct, and integrated errors in the total mass emitted of the measured species are small.

An integral part of the measurement and the prediction of mass flow is the calculated stagnation temperature history. Fig. 7 shows the calculated temperature history for bmep ≈380 kPa, 1000 rpm and 1500 rpm. The temperature history is essentially uniform and consistent with the mass flow description of blowdown followed by an incompressible phase. Comparison of other runs at different loads and speeds is not possible since the pressure initial conditions (measured with the PCB transducer at the leading spark plug) required for the model's integration can only be measured to ±5%, which is the same order as the variation in temperature histories with the conditions varied. The average temperature calculated agreed to ±10% with those measured by a thermocouple mounted in the exhaust pipe, when corrected for radiation losses and the temperature drop from the port to the thermocouple.

Radiation errors were estimated by modeling the thermocouple as a sphere and equating the radiation heat transfer to the exhaust pipe with the convective heat transfer from the exhaust gas. The temperature drop from the port to the thermocouple mounted 10 cm downstream of the orifice was calculated by assuming the enthalpy drop of the gas was equal to the enthalpy rise of the test section cooling water. Both corrections were of the order of 20–40°K.

The time resolved mass flow rate of a given species is:

$$\dot{m}_i = x_i \dot{m}_E \tag{15}$$

where x_i is the mass fraction of that species. The HC mass flow rate ($\dot{m}_{HC}$) is calculated by assuming the spectrum of unburned hydrocarbons appearing in the exhaust can be modeled by an average hydrogen to carbon ratio (s/r). The flow rate of HC is then:

$$\dot{m}_{HC} = (12 + s/r)\dot{m}_E [HC]/MW \tag{16}$$

where [HC] is in carbon atom units. The calculations presented assume s/r is equal to the hydrogen to carbon ratio of the fuel, m/n = 2.25. Curves so generated, composition histories, and results of the equivalence ratio calculations described previously are presented in Figs 8–13.*

Fig. 14 offers a simple explanation for the trends observed. Chamber ① represents the end of combustion. Along the walls are layers of unburned fuel and air resulting from the flame quenching. As the rotor rotates it begins to scrape these quench layers into a vortex with burned gas at the trailing side of the rotor. Meanwhile at ② the port opens and a large rush of burned gas leaves the chamber, dragging with it some of the quench layer from the rotor. Also at this time unburned fuel and air begins to leak into the trailing zone from the compressing chamber, and this leakage will continue through the combustion phase until combustion ceases. As time proceeds the rotor face moves away from the port ③ reducing the entrainment of rotor surface quench layer until essentially only burned gas is exhausted. Meanwhile, the vortex has been growing until

*In some composition diagrams "corners" appear near $\theta = 270°$ (bdc). They are assumed to exist since flow rates are small enough during reverse flow that significant compositional changes will not occur until flow is again out of the engine.

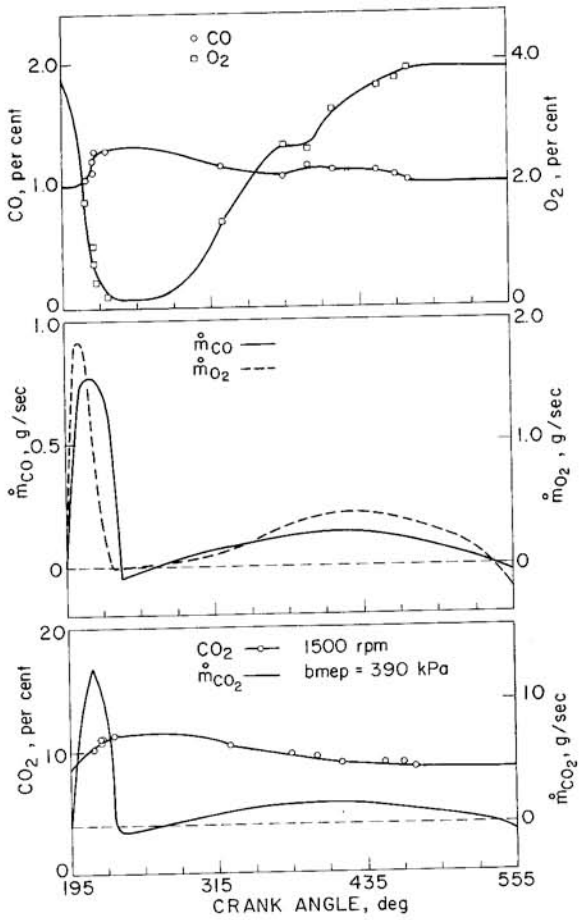

Fig. 8 – Time resolved exhaust concentrations and mass flow rates of CO, CO_2, and O_2 at 1500 rpm and bmep = 390 kPa

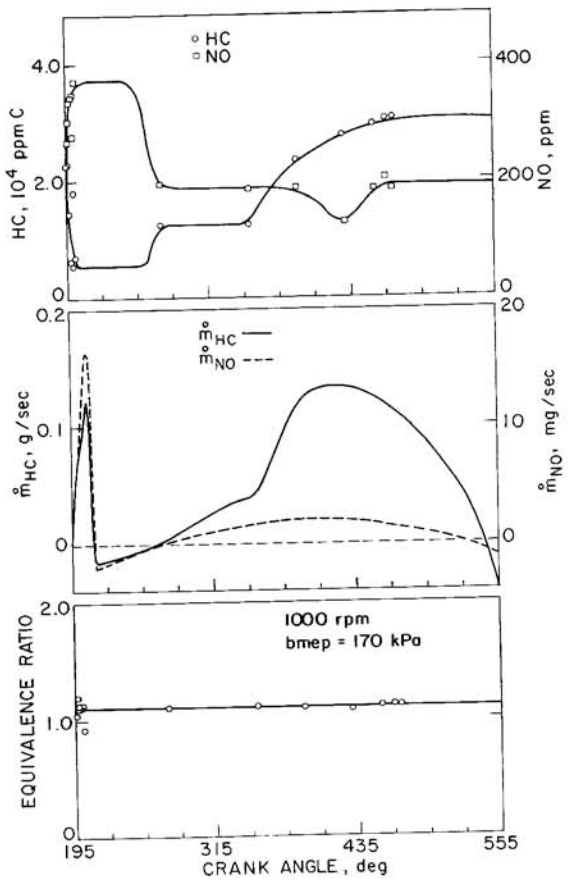

Fig. 10 – Time resolved exhaust concentrations and mass flow rates of HC and NO and time resolved exhaust equivalence ratio at 1000 rpm and bmep = 170 kPa

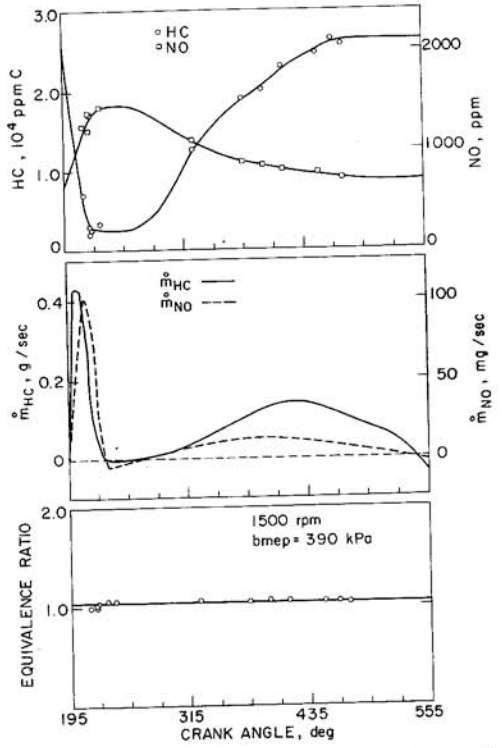

Fig. 9 – Time resolved exhaust concentrations and mass flow rates of HC and NO and time resolved exhaust equivalence ratio at 1500 rpm and bmep = 390 kPa

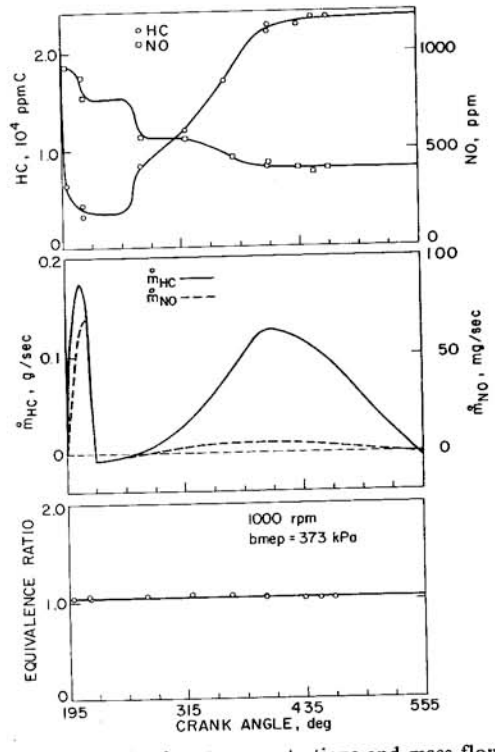

Fig. 11 – Time resolved exhaust concentrations and mass flow rates of HC and NO and time resolved exhaust equivalence ratio at 1000 rpm and bmep = 373 kPa

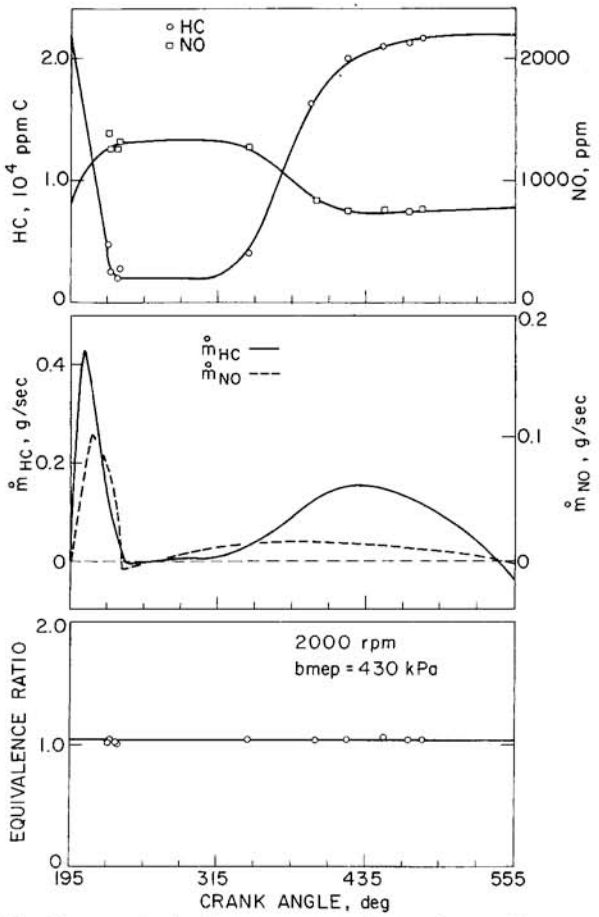

Fig. 12 – Time resolved exhaust concentrations and mass flow rates of HC and NO and time resolved exhaust equivalence ratio at 2000 rpm and bmep = 430 kPa

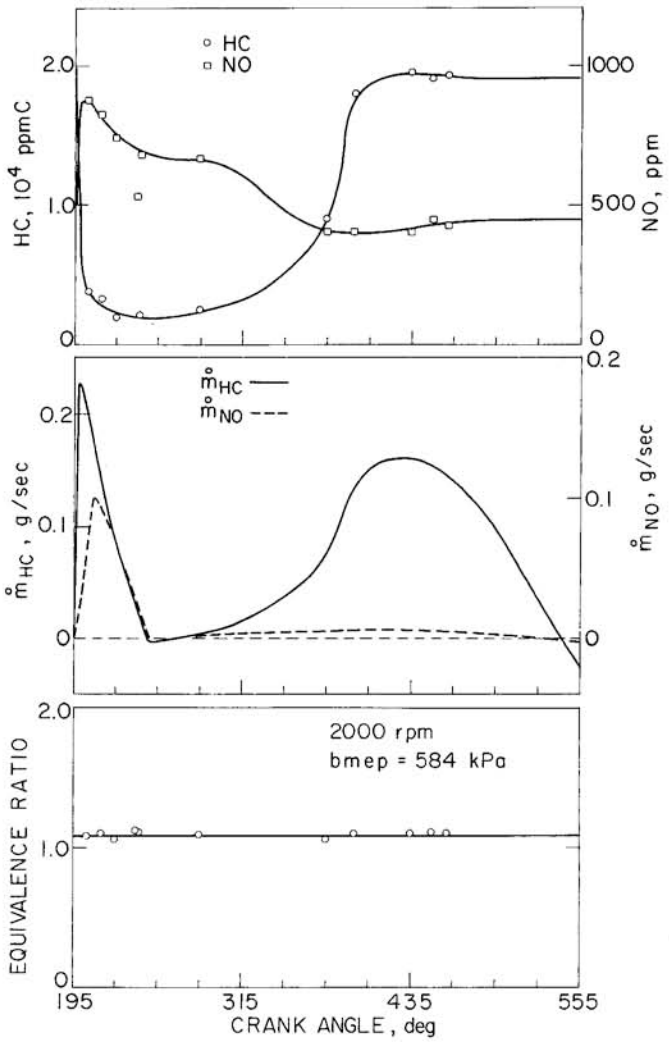

Fig. 13 – Time resolved exhaust concentrations and mass flow rates of HC and NO and time resolved exhaust equivalence ratio at 2000 rpm and bmep = 584 kPa

at ④ it is of sufficient size to be exhausted, marking the transition from a leading exhaust gas to a trailing exhaust gas.

Thus the composition of the exhaust gas is essentially in two phases: first a leading gas (burned gas and entrained boundary layers) characterized by high concentrations of NO and low concentrations of HC and O_2, followed by a trailing gas (burned gas, scraped up boundary layers, and leakage) characterized by low NO concentrations and high HC and O_2 concentrations. Nonuniformities in CO and CO_2 are small, the leading gas being slightly higher in CO and CO_2 than the trailing gas.

If the HC exhausted during blowdown results only from entrainment of the rotor quench layer then the quench area required to generate that HC should be some fraction of the rotor face area. Fig. 15 shows the mass of HC exhausted during blowdown and the total mass of HC exhausted each cycle as functions of reciprocal engine speed. The mass of HC exhausted during blowdown is speed independent and is ~0.6 mg. A quench layer covering 1-1/2 rotor areas would be required to provide this mass of HC. The discrepancy results from inadequate sampling resolution since, prior to the port opening, there is a high HC concentration gas sitting between the sampling valve and the exhaust port. The mass of HC in this volume (~.4 mg) is speed independent since the HC concentration of the trailing gas does not depend much on speed. Thus apparently only about 1/3 of the blowdown HC passing the sampling station comes from entraining the rotor quency layer. The entrained HC corresponds to quency HC from about 1/2 the rotor face area.

Were the trajectory corrections able to unravel this mixing of leading gas with the trailing gas between the port and sampling valve, it would be clear that none of the trailing gas is exhausted during blowdown. Previous analysis of the HC sources in the Wankel (3) showed that quenching sources were independent of engine speed while leakage contributions varied almost linearly with reciprocal engine speed. Since most of the leading gas is exhausted during blowdown and the blowdown HC is speed independent it follows that there is no leakage in the leading gas.

An attempt to quantify the process depicted in Fig. 14 was undertaken by assuming that in order of magnitude the growth in vortex volume is:

$$\frac{dV}{dt} = \frac{\partial V}{\partial x}\frac{dx}{dt} + \frac{\partial V}{\partial p}\frac{dp}{dt} + \frac{\partial V}{\partial m}\frac{dm}{dt} \qquad (17)$$

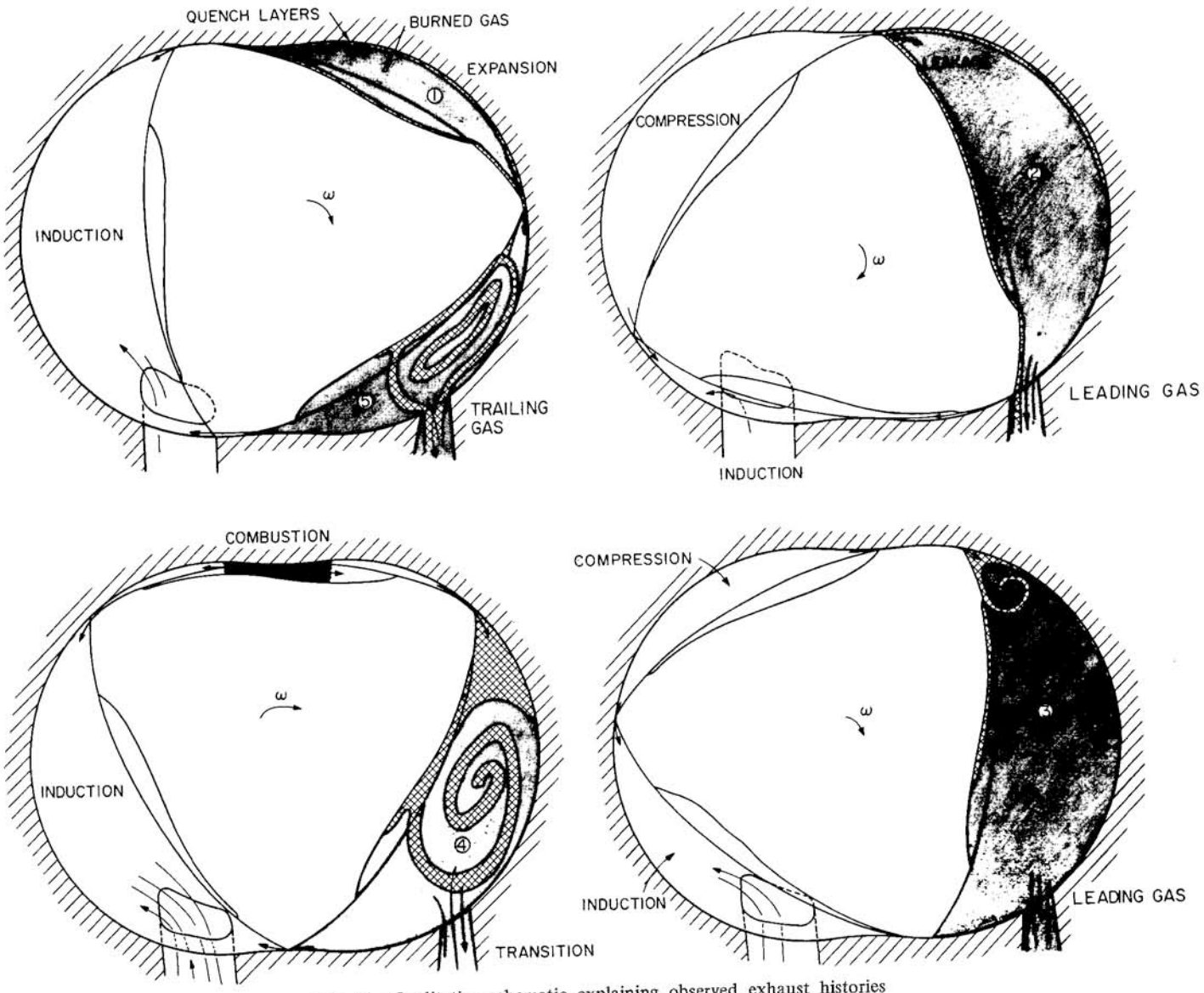

Fig. 14 – Qualitative schematic explaining observed exhaust histories (explanation in text)

where:

V = vortex volume
x = distance traveled by apex seal
dm = incremental mass addition due to leakage

The first term is evaluated from experimental data obtained by Tabaczynski (14) in a piston-cylinder geometry, while the change due to a pressure change is assumed to be an adiabatic expansion, and the leakage is assumed to add volume in direct proportion to leakage volume.

Assuming the vortex begins growing when combustion ceases, Eq. 17 has been integrated. It predicts that the leakage suppresses the vortex growth until the leakage changes sign (during blowdown) and is into the chamber. From that time the process is incompressible and thus only the first and third terms of Eq. (17) are important.

From concentration data it appears the vortex is exhausted at a crank angle of about 360 deg. There is evident a slight speed dependence, the vortex being exhausted later at the higher speeds. Assuming that the vortex volume is that volume between the exhaust port and the trailing apex at $\theta = 360$ deg then the vortex volume is about 300 cm^3.

The model, however, predicts a volume on order of magnitude too small. Clearly the process is not as simple as Eq. 17 suggests. Eq. 17 models only the scraping by the apex seal; however, the side seals are also scraping up boundary layers. From arguments presented in Appendix A it is clear that side seal vortices are volumetrically the same magnitude as that of the apex seal, and their neglect cannot account for the order-of-magnitude discrepancy previously noted.

The significance of the discrepancy is not clear since many assumptions are implicit in the analysis. There may be a large scale recirculating flow in the chamber established by the flow from the trailing part of the chamber to the leading portion when the rotor is near tdc. Such a flow can in principle continuously entrain the vortices as they grow. It is not known how the leaning angle of the apex seal affects the scraping or

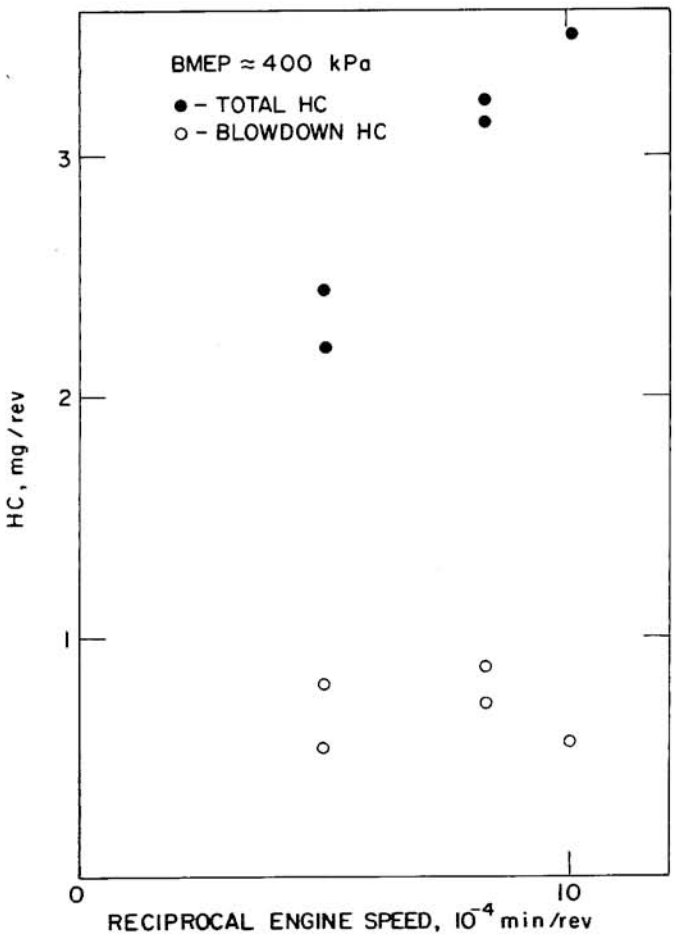

Fig. 15 – Measured blowdown HC and total HC exhausted per cycle versus reciprocal engine speed

how leakage into the vortex affects its stability. Does leakage really suppress vortex growth prior to blowdown? Where does the vortex really start? Furthermore while the leakage model (3) may be adequate for predicting average leakage behavior it may at times be far removed from instantaneous behavior. It has been suggested that housing distortions cause significant leakage, and of course the distortion pattern is not uniform around the housing. The geometry of the engine dictates that the leakage area vary as the leaning angle of the seal changes; this study used a constant effective area of 1 mm^2/chamber.

Further study is warranted toward understanding the fluid mechanics governing the exhaustion of the trailing gas since the process directly controls the fraction of HC which is exhausted. Assuming that at the end of the exhaust process there is only trailing gas left in the chamber, then there is ~0.25 mg of HC within the chamber. In comparison to the total HC exhausted, Fig. 15 shows that about 90% of the HC formed is exhausted. In contrast it has been estimated that about 2/3 of the HC formed in a piston engine is exhausted (15). The fraction exhausted can be reduced by delaying exhaustion of the trailing gas since then the HC in the residual gas will be at a maximum.

Theoretical calculations of the NO gradient in the burned gas, assuming no burned gas mixing, predict frozen concentrations which are an order-of-magnitude higher in the first elements burned than in the last burned (3). Here only a 2:1 gradient has been measured in the exhaust.

The fact that the leading gas is on the average higher in NO than the trailing gas means that, on the average, the leading gas burns earlier in the cycle than the trailing gas. This is consistent with experimental observations (4,5) that the flame is assisted in the direction of rotation and impeded in the direction opposite rotation.

Recognizing that the sampling resolution is low in the leading gas and that the trailing gas is mixed by the vortices generated about mutually perpendicular axes by the apex seal and side seals, the measured NO gradient in the exhaust shows that mixing between burned elements is incomplete.

Yamamoto et al (2) claim that the air-fuel ratio in the trailing zone of the combustion chamber is inclined to be rich due to rotation of the combustion space—that is, the trailing gas burns richer than the leading gas. Heuristic arguments presented in Appendix B indicate only one likely source of a stratified charge: concentration gradients across the inlet port at low speeds. The exhaust analysis shows no evidence of a stratified combustion.

The discrepancy noted (6) between measured CO and predicted CO levels as functions of equivalence ratio can result from deviations from the mean equivalence ratio at length scales approaching the microscale (16) and/or from freezing of reactions in the kinetics governing CO formation (17). For lean mixtures, quency generated CO may be important in determining exhaust levels.

CONCLUSIONS

1. There is no evidence of a stratified combustion.
2. There are significant nonuniformities in the exhaust concentrations of NO, HC, and O_2.
3. The exhaust mass flow from the engine is in two phases: a leading gas composed of burned gas and entrained boundary layers; a trailing gas composed of burned gas, leakage, and rolled up boundary layers.
4. Leading gas exhausted during blowdown mixes with the trailing gas in the exhaust port.
5. Exhaust concentrations of CO and CO_2 are essentially uniform, being only slightly higher in the leading gas.
6. The NO history is consistent with experimental observations of other investigators that the leading gas on the average burns earlier than the trailing gas.
7. The fluid mechanics governing the exhaustion of the trailing gas are significantly different than in a piston engine. This is responsible for a larger fraction of the HC formed in the Wankel to be exhausted relative to a piston engine.

ACKNOWLEDGMENTS

This work was supported in part by the National Science Foundation under Grant No. GK-15409 and in part by GMC.

REFERENCES

1. F. V. Bracco and W. A. Sirignano, "Theoretical Analysis of Wankel Engine Combustion," Combustion Science and Technology, Vol. 7 (1973), pp. 109–123.

2. K. Yamamoto, T. Muroki, and T. Kobayakawa, "Combustion Characteristics on Rotary Engines," SAE #720357.

3. G. A. Danieli, C. R. Ferguson, J. B. Heywood, and J. C. Keck, "Predicting the Emissions and Performance Characteristics of a Wankel Engine," SAE #740186.

4. K. Yamamoto and T. Kuroda, "Toyo Kogyo's Research and Development on Major Rotary Engine Problems," SAE #700079.

5. I. W. Froede, "James Clayton Lecture–Recent Developments in the NSU Wankel Engine," Proceedings of the Institute of Mechanical Engineers, Vol. 180 (pt. 2A) (London 1965–66), p. 279.

6. K. Yamamoto, "Rotary Engine." Toyo Kogyo, Japan, 1969, p. 137.

7. W. A. Daniel and J. T. Wentworth, "Exhaust Gas Hydrocarbons–Genesis and Exodus," SAE #486B.

8. R. J. Tabaczynski, J. B. Heywood, and J. C. Keck, "Time-Resolved Measurements of Hydrocarbon Mass Flowrate in the Exhaust of a Spark-Ignition Engine," SAE #720112.

9. R. S. Benson and E. L. Shaffie, "Non-Steady Flow Through a Square-Edge Orifice in a Pipe." Jrl. Mech. Eng. Sci., Vol. 7, No. 4 (1965) pp. 483–495.

10. Fluid Meters–Their Theory and Application." American Society of Mechanical Engineers, New York, 1959.

11. R. J. Tabaczynski, "Time-Resolved Hydrocarbon Emission Measurements in the Exhaust of a Spark Ignition Engine." Ph.D. Thesis, Dept. of Mech. Eng., M.I.T., June 1971.

12. R. S. Spindt, "Air-Fuel Ratios from Exhaust Gas Analysis." SAE #650507.

13. A. H. Shapiro, "The Dynamics and Thermodynamics of Compressible Fluid Flow." Vol. II, New York: Ronald Press, 1954, p. 929.

14. R. J. Tabaczynski, D. P. Hoult, and J. C. Keck, "High Reynolds Number Flow in a Moving Corner." Jrl. Fluid Mech., Vol. 42 (1970), pp. 249–255.

15. W. A. Daniel, "Why Engine Variables Affect Exhaust Hydrocarbon Emission," SAE Transactions, vol. 79 (1970), paper 700108.

16. H. Tennekes and J. L. Lumley, "A First Course in Turbulence." Cambridge, Mass.: M.I.T. Press, 1972.

17. M. Delichatsios, "The Kinetics of Carbon Monoxide Emissions From an Internal Combustion Engine." S.M. Thesis, Dept. of Mech. Eng., M.I.T., May 1972.

18. C. F. Taylor and E. S. Taylor, "The Internal Combustion Engine." Scranton, Pa.: International Textbook Co., 1970, p. 421.

19. L. Prandtl, "Essentials of Fluid Dynamics." New York: Hafner Publishing, 1952, p. 328.

20. R. D. Ingebo, "Atomization, Acceleration, and Vaporization of Liquid Fuels." Sixth Symposium (International) on Combustion, Combustion Institute, 1957, pp. 684–687.

21. R. A. Castleman, Jr., "The Mechanism of the Atomization of Liquids." Bureau of Standards Journal of Research, Vol. 6 (December 27, 1930), pp. 369–376.

22. W. Rohsenow and H. Choi, "Heat, Mass and Momentum Transfer." N.J.: Prentice Hall, 1961, p. 418.

APPENDIX A

SIDE SEAL VORTICES RELATIVE TO THE APEX SEAL VORTEX

Eq. 17 models only the scraping by the apex seal; however, the side seals are also scraping up boundary layers. The relative importance of the two can be estimated by the highly idealized analog depicted in Fig. A1. The real engine may be related to the idealized model by considering L/b to grow from zero at tdc to L/b ≈ 3/2 at bdc to L/b ≈ 3 at the next tdc. (L/b ≈ 3 is the ratio of rotor length to width for the Toyo Kogyo series 10A engine.)

Fig. A1 shows a straight vane rotating between two plates in a cylindrical housing. The seals are perfect and the cylinder vented to the atmosphere so that the process is incompressible. The vane rotates at constant angular velocity so that seal speeds depend only on the radial coordinate, r.

For any differential length of seal, the area scraped up can be represented by an equation of the form (14):

$$A = CU_w^{\alpha} t^{\beta} \qquad \text{(A-1)}$$

where U_w is the speed of that differential seal length, t is time, and the constants C, α, and β depend upon the vortex's stability.

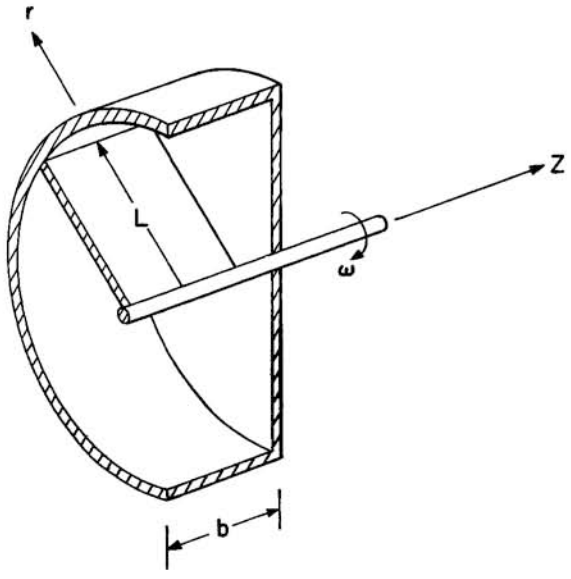

Fig. A1 – Idealized analog to evaluate relative magnitude of side seal vortex rollup versus apex seal vortex rollup

The volume scraped up by the apex seal is then:

$$V_A = \int_o^b C U_{w_A}^{\alpha} t^{\beta} dz = C U_{w_A}^{\alpha} t^{\beta} b \qquad (A\text{-}2)$$

since U_{w_A} is not a function of the coordinate, Z. Likewise the volume scraped up by side seals is:

$$V_s = 2 \int_o^L C U_{w_s}^{\alpha} t^{\beta} dr \qquad (A\text{-}3)$$

but now U_{w_s} is a linear function of the radial coordinate, r:

$$U_{w_s} = \frac{r}{L} U_{w_A} \qquad (A\text{-}4)$$

Substitution into Eq. A-3 leads to:

$$V_s = \frac{2}{\alpha + 1} C t^{\beta} U_{w_A}^{\alpha} L \qquad (A\text{-}5)$$

The ratio of side seal scraped volume to apex seal scraped volume is then:

$$\frac{V_s}{V_A} = \frac{2}{\alpha + 1} \frac{L}{b} \qquad (A\text{-}6)$$

For the engine at hand $(L/b)_{bdc} \approx 3/2$, thus for turbulent vortices ($\alpha = 2$) $V_s/V_A = 1$ and for stable vortices ($\alpha = 1$) $V_s/V_A = 1.5$. From these simple arguments it is clear that side seal vortices are volumetrically the same magnitude as the apex seal and their neglect cannot account for the order-of-magnitude discrepancy previously noted.

APPENDIX B

DROPLET DYNAMICS AT THE CARBURETOR AND INTAKE MANIFOLD

The time resolved exhaust equivalence ratios show no evidence of any large scale stratification. That conclusion can be supported in part by an order-of-magnitude analysis which looks for sources of stratification.

At 2000 rpm and wide open throttle the fuel is delivered to the air in the main metering circuits of both the primary and secondary venturi of the 4-barrel carburetor.

There are three venturi staged on the primary side and two on the secondary side. For mixture control a small amount of air is allowed to bleed into the fuel prior to injection into the high velocity airstreams at the venturi. The carburetor atomizes the fuel and mixes it with the air in two independent circuits and delivers the mixture through two ports to the inducting chamber.

A rough estimate of the air velocity, V_a, at the point of fuel injection may be made by equating the static pressure at that point to that required to delivery the measured fuel flow. See for example the model of a simple carburetor in Ref. 18. For the aforementioned conditions $V_a \approx 50$ m/s.

Prandtl (19) argues that the maximum drop diameter that can exist in an airstream is:

$$d_{MAX} \approx 7.7 \frac{\sigma}{\frac{1}{2}\rho_a V_a^2} \qquad (B\text{-}1)$$

where σ is the surface tension of the liquid drop and ρ_a is the air density.

Once formed the drop accelerates such that the relative velocity between the drop and the surrounding air decays exponentially in a time:

$$\tau_a \approx \frac{4}{3} \frac{\rho_L}{\rho_a} \frac{1}{C_{d_o}} \frac{d}{V_a} \qquad (B\text{-}2)$$

where:

ρ_L = drop density
C_{d_o} = initial drag coefficient
d = drop diameter

The acceleration described based on Stoke's Law is an upper bound since experimentally it is observed that the drag coefficient for accelerating drops is larger than that of a hard sphere in a steady flow (20).

The drop in the carburetor may be assumed describable as a sphere and accelerating according to Eq. B-2 if its formation time is short compared to its time of residence in the carburetor, τ_{carb}. The formation time (21) is approximately:

$$\tau_F \approx \frac{3}{5}\left(\frac{\rho_L d^3}{\sigma}\right)^{1/2} \ell n\left(\frac{d}{4 \times 10^{-5}\ \text{cm}}\right) \qquad (B\text{-}3)$$

Ref. 22 cites the following equation for mass transfer from a sphere:

$$Sh = 2.0\left[1.0 + 0.276\, R_{e_d}^{1/2} S_c^{1/3}\right] \qquad (B\text{-}4)$$

where:

Sh = Sherwood number
R_{e_d} = Reynolds number
S_c = Schmidt number

The evaporation time is then:

$$\tau_e = \frac{d^2 \rho_L}{4 Sh D \Delta C_F} \qquad (B\text{-}5)$$

where:

D = mass diffusivity
ΔC_F = concentration of fuel vapor at drop surface minus concentration of fuel vapor in free stream

Calculations of the characteristic times for a drop of maximum diameter yielded:

$$d_{max} \approx 30\ \mu m$$

$$\tau_{carb} \approx 3\ ms$$

$$\tau_a \approx 2\ ms$$

$$\tau_F \approx 0.07\ ms$$

$$\tau_e \approx 8\ ms$$

Thus it appears that the drop can be represented as a sphere in the carburetor, that it is accelerated to the mainstream velocity in the carburetor, and that evaporation reduces its surface area by the ratio $\tau_e/\tau_{carb} = 3/8$. The d_{max} leaving the carburetor is thus 20 μm, and 20% of the mass of the largest drops evaporates.

Experimentally it was estimated that 40% of the fuel evaporated in the carburetor. This was measured as a drop in air temperature through the carburetor of 14°K. Thus the order-of-magnitude analysis is consistent with at least one measurement.

After the carburetor the drops move with zero relative velocity so that the Sherwood number is 2.0 and $\tau_e \approx 10$ ms. The residence time in the intake manifold $\tau_1 \approx 7$ ms is long enough to evaporate the remaining drops prior to delivery to the engine.

At lower engine speeds and part-throttle conditions the droplet dynamics are complicated by the now more complicated flow in the carburetor. Consider as a worst case 1000 rpm and bmep = 173 kPa. Now all the airflow is through the primary side of the carburetor and most of the fuel is injected by the idling circuit below the throttle plate. The air velocity, $V_a \approx 20$ m/s, and density, $\rho_a \approx 0.8$ mg/cm^3, are such that the maximum drop diameter that can stably exist is $d_{max} \approx 250$ μm. It is doubtful that drops this large are formed since the fuel is premixed with air prior to injection, and furthermore it is injected after the throttle where the flow is violently turbulent.

At low speeds and part-throttle conditions it is thus not inconceivable that drops exist which are large enough to collide with the walls of the intake manifold (which is curved) and form a film. The walls of the manifold are at a temperature near 370°K so that the film is boiling. This process could clearly set up a concentration gradient across the intake manifold.

The drops which are able to follow the flow and avoid collision with the walls are small enough to evaporate in $\tau_1 \approx 7$ ms, the residence time of the air in the intake manifold.

The exhaust analysis, together with the realization that mixing between burned elements prior to sampling is incomplete, indicates that any nonuniformities in the unburned gas are smoothed prior to ignition to a scale small compared to chamber dimensions.

Society of Automotive Engineers, Inc.
400 COMMONWEALTH DRIVE, WARRENDALE, PA. 15096

16 page booklet.

Printed in U.S.A.